ADVANCED FUNCTIONAL MATERIALS
www.afm-journal.de

Rapid and Controllable Digital Microfluidic Heating by Surface Acoustic Waves

Richie J. Shilton, Virgilio Mattoli, Marco Travagliati, Matteo Agostini, Andrea Desii, Fabio Beltram, and Marco Cecchini**

Fast and controllable surface acoustic wave (SAW) driven digital microfluidic temperature changes are demonstrated. Within typical operating conditions, the direct acoustic heating effect is shown to lead to a maximum temperature increase of about 10 °C in microliter water droplets. The importance of decoupling droplets from other on-chip heating sources is demonstrated. Acoustic-heating-driven temperature changes reach a highly stable steady-state value in ≈3 s, which is an order of magnitude faster than previously published. This rise time can even be reduced to ≈150 ms by suitably tailoring the applied SAW-power excitation profile. Moreover, this fast heating mechanism can lead to significantly higher temperature changes (over 40 °C) with higher viscosity fluids and can be of much interest for on-chip control of biological and/or chemical reactions.

1. Introduction

Surface acoustic waves (SAWs) represent a very useful platform to successfully address a number of fluidic processes otherwise difficult to control when fluid volumes are reduced to the microscale.[1] Examples of complex microfluidic operations that SAWs excel at are mixing,[2–5] particle manipulation,[3,6–8] atomization,[9–11] droplet actuation,[9,12,13] fluid pumping,[14–22] and centrifugal microfluidics.[23,24] Within the wider context of digital microfluidics,[25,26] SAWs can be successfully used for fluid manipulations in both droplet emulsions in channels,[27–29] as well as free droplets.[1–5,9,10] SAWs can provide a variety of microfluidic functions—often significantly more rapidly than other methods—ultimately owing to the large momentum transfer upon fluid–SAW interaction.[30] When SAWs propagating on a substrate surface meet a fluid droplet or stream on the same substrate, owing to the sound–velocity mismatch between substrate and fluid, SAWs will radiate acoustic energy into the fluid. This will induce a pressure wave and drive a steady-state flow known as acoustic streaming, the basis for the gamut of possible SAW microfluidic operations. At the same time, however, the viscous dissipation of the acoustic energy into the fluid can generate a heating effect.[31]

This heating effect is a much-discussed issue in SAW-driven microfluidics and questions surrounding the problem of fluid heating are continually arising. How much will the dissipation of the acoustic wave into a droplet raise its temperature? Will any temperature rise be enough to negatively affect biological samples or even evaporation rates? This is especially of concern in the case of free-droplets where a systematic study of fluid-heating effects would be desirable over the typical SAW-microfluidic operational frequency and power ranges. At the same time, it is interesting to understand to which extent any microfluidic heating effects can actually be positively exploited to enhance biological or chemical reactions in lab-on-a-chip devices when desired.

To date, only few studies investigated SAW thermal effect in microfluidics. The first reported characterization of SAW-driven liquid heating effects was carried out by Kondoh et al. in 2005 and further expanded upon in 2009.[31–33] In these experiments, the authors demonstrated that the primary source of fluid heating is, in fact, the radiated acoustic wave, with temperature changes being strongly dependent on input power and fluid viscosity. It was not clear, however, if droplet heating was isolated from heating effects occurring at the interdigital transducer (IDT). The latter can significantly heat up the substrate—and through it the droplet on its surface—if not properly controlled. In 2006, Beyssen et al. reported similar results using comparable experimental conditions, further quantifying the effect of fluid viscosity on temperature changes and uniformity.[34] In 2009, Kulkarni et al. showed the possibility to use this heating mechanism as an energy source for synthetic chemistry in digital microfluidic systems.[35] More recently, Roux-Marchand et al. further investigated the temperature uniformity within viscous glycerol droplets and found decreased uniformity at high SAW powers but did not discuss absolute temperature changes.[36] As a recent application of acoustic microdroplet heating, Reboud et al. demonstrated polymerase chain reactions (PCRs) in an oil-covered droplet.[37]

Dr. R. J. Shilton, M. Travagliati, M. Agostini
Center for Nanotechnology Innovation@NEST
Istituto Italiano di Tecnologia
Piazza San Silvestro 12, 56127 Pisa, Italy
E-mail: richard.shilton@iit.it
Dr. V. Mattoli, A. Desii
Center for Micro-BioRobotics @SSSA
Istituto Italiano di Tecnologia
via R. Piaggio 34, Pontedera 56025, PI, Italy
M. Travagliati, M. Agostini, Prof. F. Beltram, Dr. M. Cecchini
NEST, Scuola Normale Superiore and Istituto Nanoscienze-CNR
Piazza San Silvestro 12, 56127 Pisa, Italy
E-mail: marco.cecchini@nano.cnr.it

DOI: 10.1002/adfm.201501130

These authors extended Hodgson et al.'s idea of coupling a SAW substrate to a disposable superstrate in which a lamb wave was generated[38] that in turn interacted with the fluid on the superstrate. While these studies demonstrate the interest and potential of SAW-driven microfluidic heating, none of them addressed the effect of direct SAW-driven heating—decoupled from other heating sources—over the full range of frequencies and powers typically used for SAW microfluidics.

Here, we investigate SAW-driven heating in digital microfluidic systems. Droplet heating by acoustic dissipation into the fluid was carefully decoupled from spurious temperature effects produced at the IDT by directing the heat flow from the IDT toward a temperature-controlled heat sink. Droplet temperature changes were measured over the range of operating frequencies (O(10–1000 MHz)) and powers typically used for SAW-driven microfluidic functions,[39] for full characterization. This study demonstrates that acoustic heating produces relatively low-temperature changes (on the order of 10 °C or less) when working with water in standard configurations. We shall show fast timescales on the order of a few seconds to reach thermal equilibrium that are further reducible to ≈150 ms by suitable choice of the applied SAW power profile. Finally, we shall demonstrate that by changing the viscosity of the working fluid it is possible to generate larger temperature changes when desired, e.g., to drive biological or chemical reactions.

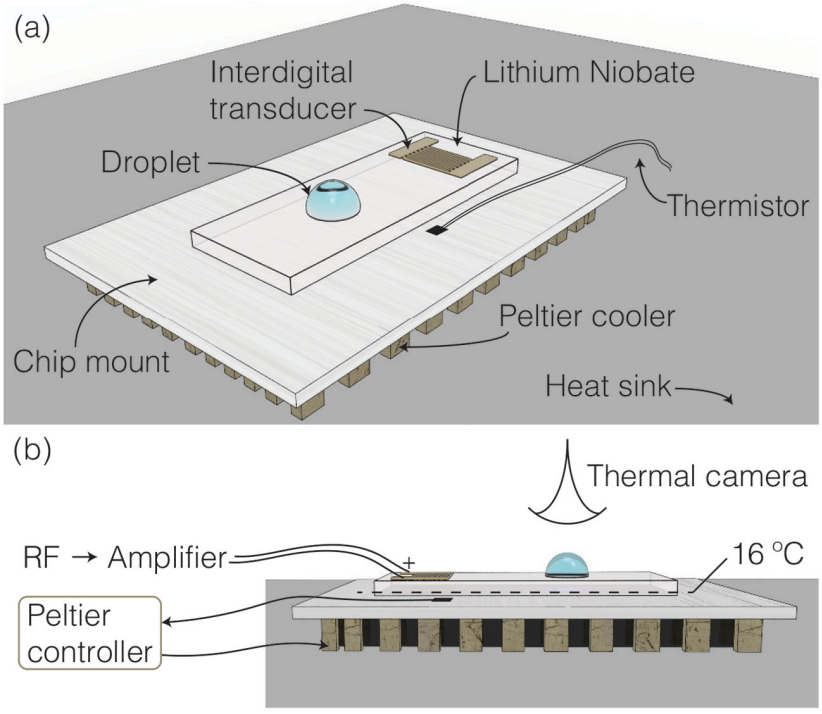

Figure 1. a) Experimental schematics, with the thermal camera mounted from above (not shown). The setup consists of four parts: the gold-patterned LN SAW chip with hydrophilic wells; an aluminum chip mount (with thermistor temperature sensor for Peltier controller feedback); a Peltier cooler; and a large heat sink (aluminum breadboard). Thermal gel-gap pad (RS components #7074764) was placed in between each layer to assist in heat transfer (not shown). b) Operational pseudo-block-diagram. Schematics are not to scale.

2. Materials and Methods

The SAW devices used in these experiments were fabricated on 128° Y-cut, X-propagating lithium niobate (LN) substrates. 100 nm thick straight-finger gold IDTs were patterned onto the LN with a 10 nm titanium adhesion layer, via optical (50–400 MHz devices) or electron-beam (600–900 MHz devices) lithography. The aperture of each IDT was set to 700 μm[18] and finger thicknesses, t, (where $t = \lambda_s/4$ and λ_s is the SAW wavelength) were designed so that device nominal frequencies were 50, 100, 200, 400, 600, and 900 MHz. Two devices were fabricated for each nominal frequency. Reflection coefficients were measured for each device and the actual frequencies, f, were found to be slightly lower than the nominal frequencies (measured frequencies were 47.9, 47.9, 97, 96.5, 188.2, 190.8, 369.1, 380.6, 554, 554, 819, and 817.4 MHz). SAW amplitudes, ξ, were measured for each device against SAW power using a laser Doppler vibrometer (UHF-120 Ultra High Frequency Vibrometer, Polytec, Germany); a 25-point line average was used in front of the unloaded droplet position to account for any variation in the SAW amplitude. Other device properties were constant between devices. For consistent drop positioning, and for repressing droplet translation at high power, surface silanes (octadecyltrichlorosilane) were patterned onto the chips at the final stage to form 1.5 mm diameter hydrophilic wells. A schematic of the SAW chip can be seen in **Figure 1**, and fabrication details for similar devices can be found in ref.[40].

Figure 1b shows the experimental process employed to characterize SAW-driven droplet heating. Water droplets of 1 μL volume were placed in the hydrophilic wells, ≈5 mm from the IDT along the center of the SAW path. In order to change droplet temperature, we applied high-frequency sine waves to the IDTs at varying power levels using an RF generator (MXG Analog Signal Generator N5181A, Agilent Technologies) connected to an amplifier (ZHL-5W-1, MiniCircuits). The RF was applied for 10 s, long enough for the temperature to rise and stabilize. We measured droplet temperature changes over time with an infrared camera (FLIR A655sc with macroscopic lens). Each video captured temperature rise and fall, as well as a few seconds of prebuffer data. For each frequency, we measured the temperature change in five different droplets at five different power levels for two different chips. For each of these videos, we exported the time series of the average droplet temperatures. The time series in each case were fit with an exponential curve of the form $T(t) = Tss(1 - et/\tau)$, where $T(t)$ is the temperature change over time, Tss gives the steady-state temperature reached, and τ is the characteristic time constant. These constants were used to compare SAW-driven temperature changes and time scales across experimental conditions. As an alternative to varying SAW power, we also varied the duty cycle using

DOI: 10.1002/adfm.201501130

pulse-width modulation of SAW excitation with a 1 ms period. In order to investigate the effect of increasing viscosity, water droplets were replaced by glycerol–water mixtures with no changes in the experimental procedures. Droplets were tested with glycerol in water percentages by volume of 0%, 50%, 80%, and 100%, giving initial dynamic viscosities (at 16 °C) of ≈1.1, 10, 121, and 2067 cP, respectively.[41] For mixing experiments, mixing data were obtained by adding 10% dye in 1 µL water microdroplets and generating mixing via SAW devices over the frequency and power ranges considered in all experiments. Mixing efficiency was determined by computing a normalized mixing index over time from microscopy videos of the process, using the equations described in ref.[4].

In all experiments, SAW devices were placed atop a temperature-controlled aluminum chip carrier in order to facilitate heat removal from the IDTs, away from the droplet (the thermal conductance of aluminum is much higher than that of LN). The aluminum chip carrier (and therefore the SAW device) was held at a constant temperature (16 °C) with a Peltier cooler and Peltier control unit (Thorlabs TED350), with feedback from an attached thermistor. When no droplets were placed on the SAW device, the region where the droplet was to be placed was found to remain at a constant temperature when the SAW was generated, thus confirming the absence of spurious heating sources at this location (Figure S1, Supporting Information). With this setup, in contrast to previous studies, any measured droplet temperature changes are a direct result of the SAW-fluid interaction alone.

In order to decrease the time required to bring the droplet to its equilibrium temperature, we also explored a different SAW power excitation profile and added a short high-power pulse before the steady-state excitation. Glycerol droplet (1 µL) temperature changes were monitored as a result of a SAW power of 20 dBm when this was preceded by an initial power pulse of 30, 26, 24, and 22 dBm for 130 ms, 400 ms, 720 ms, and 1.4 s, respectively. These power–time combinations were chosen in order to reach the required steady-state temperature. The total heating time was set to 10 s in all cases and compared with the standard case with no initial additional power burst.

3. Results and Discussion

Figure 2 shows thermal images taken from representative SAW-driven heating experiments with a 1 µL water droplet. In this case, SAW-driven heating is shown for two excitation power values: 20 dBm and 23 dBm, both at 100 MHz resonant frequency (the images are qualitatively similar to other SAW power and frequency values; see Video in the Supporting Information). Owing to the ultrafast mixing process that occurs when SAWs impinge on fluid droplets,[4] the fluid temperature can be seen to remain highly homogenous in the whole droplet image. The standard deviation of the temperature over the droplet area was measured in each case to be below 0.2 °C, significantly less than previously seen for high-viscosity fluids and thin films.[35] These images show qualitatively that for SAW-driven water-droplet heating, steady-state temperature is reached after ≈3 s and remains highly stable for longer times. **Figure 3**a quantitatively shows the time-series plots of the change in temperature for each droplet driven by the 100 MHz SAW device at the different power levels studied (the highest two power time series being represented in Figure 2). Here, we also see quantitatively that the temperature change in each case does reach its maximum and steady-state temperature after ≈3 s, with an average characteristic time constant, $\tau = 0.65 \pm 0.06$ s. This is significantly faster than reported in previous studies where temperatures were observed to rise for up to 60 s.[31–33] We attribute those longer heating times to the IDT itself, since it behaves as an additional source of heat that can propagate through the substrate to the droplet via conduction with a much longer time scale than direct acoustic heating of the droplet via the SAW itself. This effect could be observed in our experiments also, by removing the temperature-controlled heat sink. We registered a slower poorly controlled droplet temperature rise to a higher value (Figure S2, Supporting Information). On the contrary, when SAW-driven droplet heating was decoupled from spurious substrate-mediated heating with the aluminum heat sink, we found droplet temperature changes to be lower, fast, stable, and highly reproducible. This demonstrates the often-ignored need to manage the heat produced by the RF excitation at the IDTs and isolate from it the microfluidic samples. In terms of chip design, this means that the working droplet can be placed at an arbitrary distance from the IDT itself (with consideration only for the SAW decay along the substrate), since SAWs interact with (and heat) the droplet directly.

Figure 3 also demonstrates two different methods that can be used to control the steady-state temperature reached within the droplets. Figure 3a shows increased change in temperature with increased input power to the SAW-device, whereas

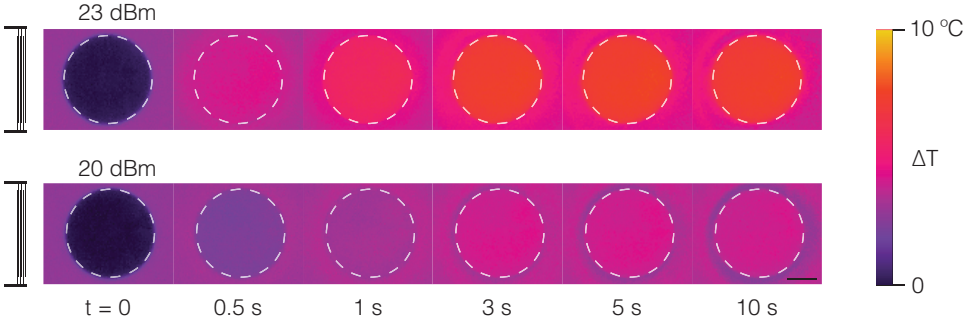

Figure 2. Thermal camera video stills of microliter droplet heating at two different input power values at 100 MHz. The color bar shows the change in temperature with applied SAW. The dashed droplet outline is added to aid visualization, and the scale bar is 500 µm.

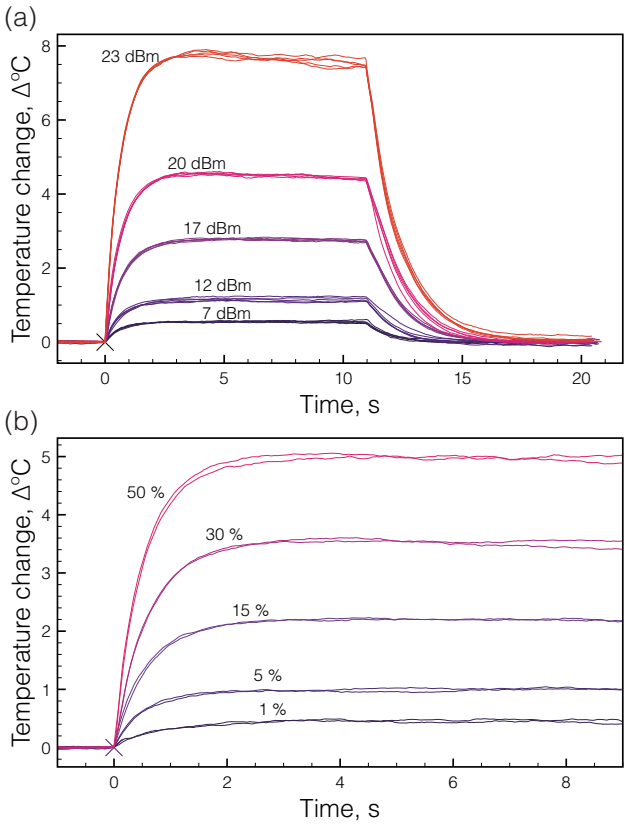

Figure 3. Droplet heating can be controlled by varying the a) input power to the device, or the b) duty cycle at constant input power (23 dBm here). In each case, steady-state temperatures are reached after ≈3 s.

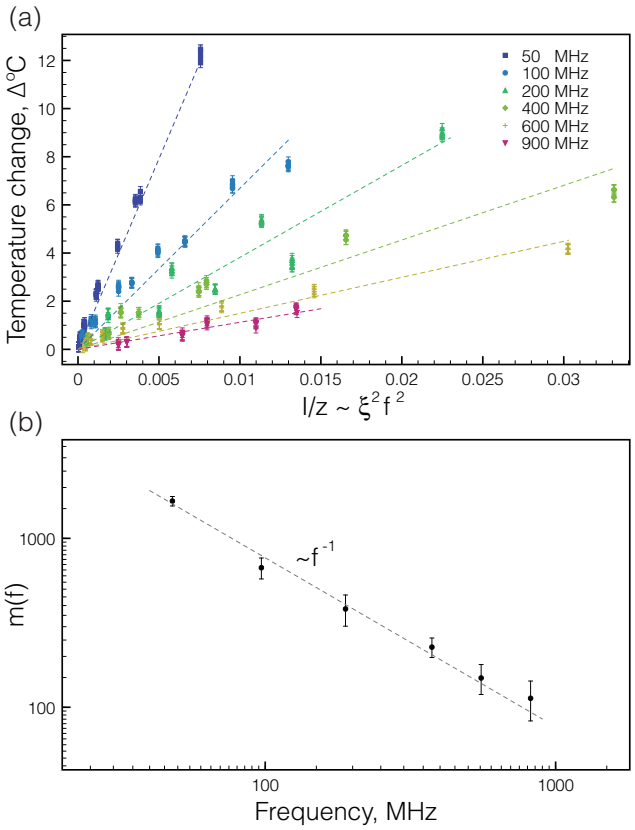

Figure 4. SAW-driven droplet heating in several devices operating from 50 to 900 MHz. Droplet temperature increase is shown to be a) linear against SAW intensity with a b) linearly decreasing gradient, $m(f)$, with increasing SAW frequency. For microliter water droplets the temperature rise measured was at most ≈12 °C, but generally significantly less.

Figure 3b shows an alternative method of controlling the temperature change by reducing the duty cycle at a set power. Both plots show the same features, with quantitatively similar time scales (in Figure 3b, the average characteristic time constant $\tau = 0.56 \pm 0.05$ s) and linearly increasing temperature changes, and can be used interchangeably to control (or reduce) digital microfluidic temperatures as required. A slightly higher spread of steady-state temperature changes can be seen at the highest power shown in Figure 3a. It is likely due to the fact that at this power the droplet begins to atomize, which may aid in heat transfer between the droplet and the surrounding air, in addition to slightly changing the droplet volume over time.

Water droplet temperature changes were next measured as driven by SAW devices with nominal frequencies from 50 to 900 MHz. The input power range was set from the lower bound, where there was a temperature change on the scale of the thermal camera noise (±0.2 °C), to the upper bound where the droplets began to atomize or translate out of the hydrophilic wells. These ranges of frequency and power values cover the typical operating range of SAW devices used in microfluidics. **Figure 4**a shows the steady-state temperature change measured for each of the experimental runs, as a function of the acoustic intensity, $I = \xi^2\omega^2 z$, (where $\omega = 2\pi f$) divided by the acoustic impedance, $z = \rho_s c_s$, which is a function of the substrate properties (density, ρ_s = 4650 kg m^{-3}, and speed, c_s = 3990 m s^{-1}, for LN) and therefore constant in all devices.[42] We see from Figure 4a that for water droplets the temperature increase via acoustic heating is linear at each frequency with respect to the acoustic intensity; however, the gradient, $m(f)$, decreases with an inverse proportionality with frequency, as shown in Figure 4b. Importantly, we see that in every case the total temperature change for microliter water droplets is below 12 °C, showing that by SAW-driven acoustic heating alone the temperature increase is quite modest: it is not likely to have a large effect on evaporation rates of free droplets.

Figure 5 shows the measured temperature change versus acoustic power into the droplet. Note that the acoustic damping length of the SAW on the substrate as it leaks into the droplet is, for each device, much less than the droplet diameter ($x_s = 0.45\lambda_s (\rho_s c_s)/(\rho_f c_f)$, where ρ_f and c_f are the density and speed of the SAW in the fluid, respectively). It follows that all SAWs impinging on the droplet will be radiated into the droplet.[39,43] Therefore, we take the total SAW power into the droplet as the acoustic intensity multiplied by the area, A, as the wave propagates along the substrate surface, which is estimated as the aperture of the SAW, 700 µm, times the depth of the SAW below the substrate surface. This penetration depth scales with wavelength and is approximated here as one wavelength, λ_s. This can explain the inverse frequency relationship shown in Figure 4b, as the decrease in temperature change with

Adv. Funct. Mater. 2015,
DOI: 10.1002/adfm.201501130

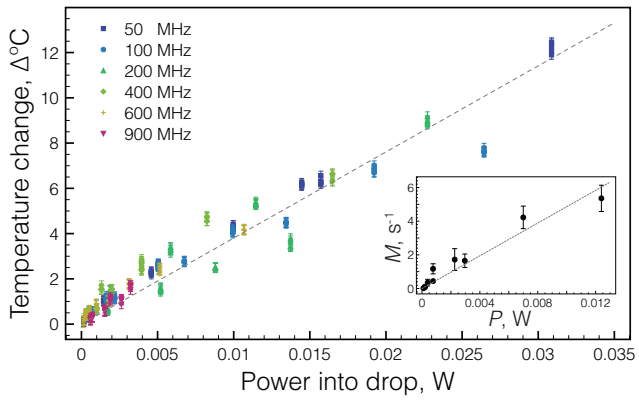

Figure 5. Droplet heating across all devices is seen to be linear with SAW power into the fluid, akin to SAW-driven mixing efficiency, *M* (inset).

increasing frequency can be attributed to the decreased total area through which the wave passes. Figure 5 shows the important result that, over the range of devices typically used for SAW microfluidics, the heating effect is linear simply with the SAW power impinging on the working fluid (with $R^2 = 0.93$). This also shows that there is negligible frequency dependence on fluid heating up to *O*(1 GHz); therefore, devices can be designed to various frequency requirements with similar fluid heating changes. This result mirrors what is seen for SAW-driven mixing efficiency (Figure 5 inset), which over the same range also shows a linear relationship with the SAW power.[39] These results can be exploited for SAW device design for highly controlled microfluidic heat and mass transport.

If temperature changes are instead desired in a microfluidic system, droplet heating can be significantly increased by increasing the viscosity of the working fluid,[31] or by embedding the working fluid (typically water) in high-viscosity droplets.[37] Viscosity can also be an important parameter when working with biological reactions, as crowding of biomolecules can lead to a higher viscosity of the working fluid. **Figure 6**a shows the temperature change time series for 100% glycerol droplets at varying input power for a 50 MHz device. Figure 6b shows the measured temperature rise for varying glycerol–water mixtures (0%, 50%, 80% and 100% glycerol by volume, with initial dynamic viscosities of 1.1, 10, 121, and 2067 cP, respectively) against SAW power for the 50 MHz device, and shows increased heating with increased viscosity. These heating time series exhibited the same qualitative features as with the water droplets in Figure 3, that is, fast temperature rises and stable steady-state temperatures, albeit much higher. In these cases of higher viscosity droplets, steady-state temperature increases of over 40 °C were attainable, which may be useful for reliable control of biological or chemical reactions in microreactors. The characteristic time constants in the time series shown in Figure 6a were found to slightly increase as the power was reduced, with $\tau = 0.62$, 0.77, 0.91, 0.98, 1.83, and 1.55 s, ordered from the highest power to the lowest. This probably stems from the longer mixing times found when the SAW power is low and fluid viscosity is high,[4] combined with the more localized acoustic streaming due again to the high viscosity. It is of note that for these droplets the temperature

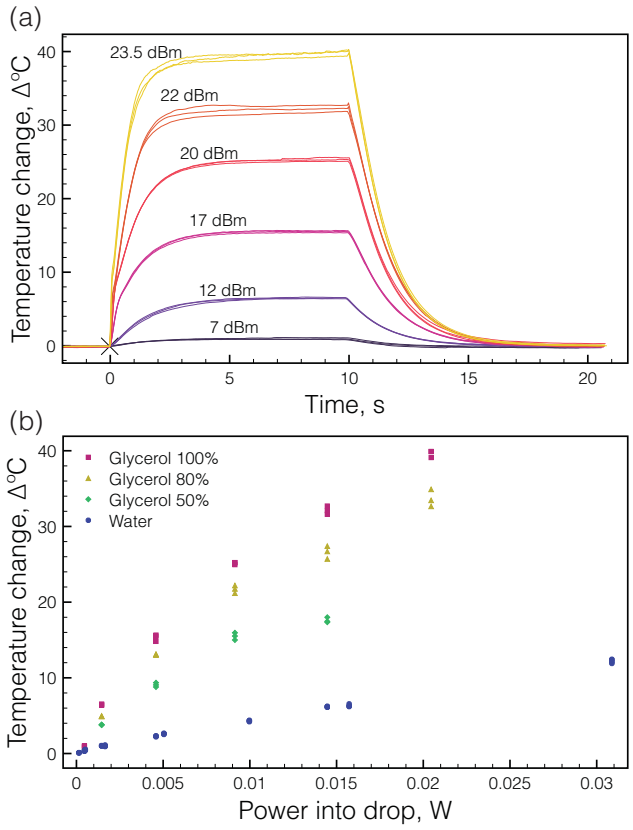

Figure 6. Droplet heating by 50 MHz SAW devices of a) 100% glycerol droplets against time at various input power values, and b) various glycerol–water mixtures against SAW power into the droplets. Glycerol percentages were 0%, 50%, 80%, and 100% by volume, with initial dynamic viscosities of ≈1.1, 10, 121, and 2067 cP, respectively.

rise is nonlinear with input power, possibly owing to the significant change in viscosity that occurs as the glycerol mixtures are heated. High viscosity SAW-driven heating also exhibited higher spatial variation of temperatures across the droplets, with temperature standard deviations qualitatively and quantitatively similar to what has been previously reported (as shown in the Video in the Supporting Information).[36] This increased inhomogeneity can be attributed to both the slower transport of fluids as the viscosity increases, as well as the greater localization of the SAW jet at the droplet front. The upper limiting case here was set by the power at which droplets began to translate out of the hydrophilic wells; so, much higher temperatures may be reached with better-confined droplets or alternate transducer design and/or arrangement.

For chemical and biological reactions in microfluidic devices, it is often important to induce thermal cycling that is both fast and highly controlled. **Figure 7** shows the temperature of a 1 µL glycerol droplet, which was cycled between typical temperatures required for PCR,[44] by applying 10 s long SAW pulses at 22.7 dBm separated by 10 s intervals. We see that the temperature changes are again very rapid, as well as reproducible with each change between the base temperature of 65.0 ± 0.1 °C and the upper temperature of 95.8 ± 0.1 °C. Temperatures required for alternative applications can be tailored by changing the

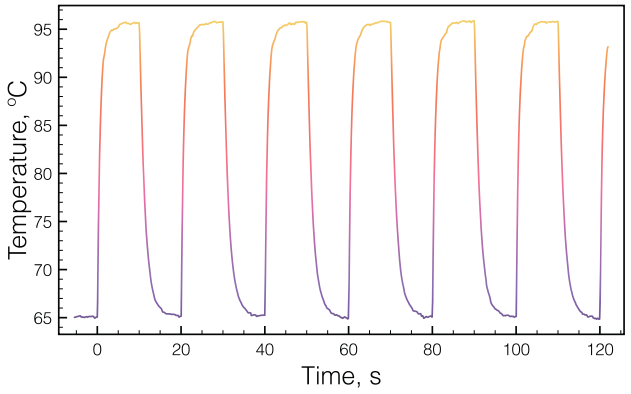

Figure 7. Temperature response of a 1 µL glycerol droplet heated via SAWs driven by a pulsed input signal (20 s period with 10 s pulse duration at 22.7 dBm) with a base substrate temperature of 65 °C.

input power (or duty cycle), as well as adding intermediate steps. Importantly, steady-state temperatures can be reached on the order of seconds, rather than minutes as previously reported,[31–33] which can be critical when rapid temperature changes are required.

It is possible to further reduce SAW-driven heating times by applying additional short high-power pulses to the steady-state excitation as seen in **Figure 8**. By adding increasingly more intense and shorter power bursts at the start of each excitation cycle, the temperature rise time was seen to decrease while preserving the steady-state temperature change. Figure 8 (upper panel) shows the temperature response to the input signals shown in the lower panel. A very fast response time, as short as ≈150 ms, to reach steady state can be seen for the highest and shortest burst power. This corresponds to a heating rate of up to 70 °C s^{-1} followed by an almost instantaneous stabilization at the steady-state temperature. The inset of Figure 8 shows the characteristic heating time constants against initial excitation power and demonstrates an inverse relationship (R^2 = 0.95) with a minimum of τ = 113 ms in the highest power case—an order of magnitude decrease in heating time. In this case, a temperature fluctuation can be seen at the initial times. We believe that this is a result of the ultrafast heating mechanism being faster than the temperature homogenization time throughout the droplet. The slightly faster cooling rate at increasing burst powers may be due to the fact that the high power bursts caused the droplets to spread slightly, leading to a greater surface area for heat transfer when the SAW is switched off. In any case, we wish to underline that not only the steady-state temperature can be changed but also even the heating rates can be tuned by varying the SAW-power profile. This is a valuable additional control that can be of use for controlling lab-on-a-chip chemical and/or biological reactions.

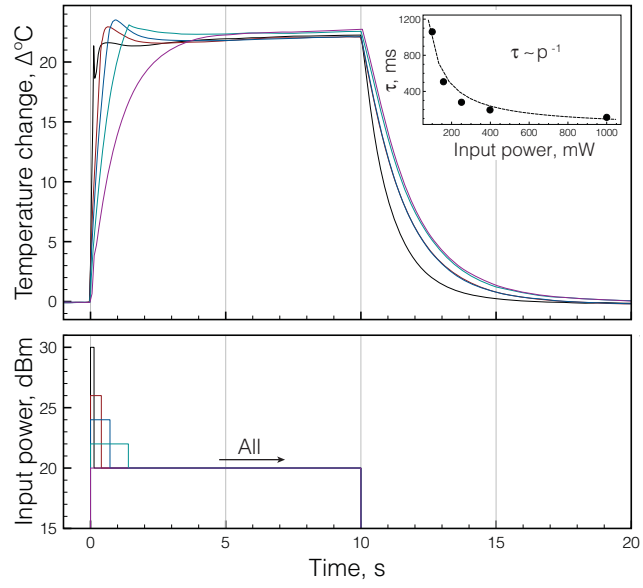

Figure 8. By adding an initial short higher-power burst to the steady-state input signal (20 dBm here), the time to reach equilibrium temperature can be significantly reduced to ≈150 ms. The upper panel shows the droplet temperature changes corresponding to the similarly colored input signal from the lower panel. The inset shows the characteristic time constants observed with the different initial input burst power tested, with the fit shown as a dashed line. The initial burst power intensities and durations were 30 dBm for 130 ms (•), 26 dBm for 400 ms (•), 24 dBm for 720 ms (•), and 22 dBm for 1.4 s (•). (•) labels the no initial burst case.

4. Conclusion

We studied SAW-driven direct microfluidic droplet heating over the range of frequency (50–900 MHz) and power (up to 25 dBm) typically used in SAW-microfluidic processes in lab-on-a-chip devices. These experiments carefully isolated the acoustic heating effects within the fluid from other heating effects by setting the SAW devices atop a temperature-controlled heat sink. Temperature changes in microliter water droplets did not exceed 12 °C, but much higher temperature changes were accessed by varying fluid viscosities. SAW-driven droplet temperature changes were found to reach steady state in ≈3 s—further reducible by an order of magnitude to 150 ms by modifying the SAW-excitation profile. This can be exploited for fast and highly stable control of chemical and biological reactions, and performed with complementary SAW-driven processes such as on-chip mixing, droplet translation, and particle separation for integrated devices.

Supporting Information

Supporting Information is available from the Wiley Online Library or from the author.

Acknowledgements

This work was in part supported by the CNR project: NANOMAX nanotechnology-based therapy and diagnostics of brain diseases NANOBRAIN.

Received: March 20, 2015
Revised: July 28, 2015
Published online:

[1] J. Friend, L. Y. Yeo, *Rev. Mod. Phys.* **2011**, *83*, 647.
[2] A. Wixforth, C. Strobl, C. Gauer, A. Toegl, J. Scriba, Z. v. Guttenberg, *Anal. Bioanal. Chem.* **2004**, *379*, 982.
[3] R. Shilton, M. K. Tan, L. Y. Yeo, J. R. Friend, *J. Appl. Phys.* **2008**, *104*, 014910.
[4] R. J. Shilton, L. Y. Yeo, J. R. Friend, *Sens. Actuators, B* **2011**, *160*, 1565.
[5] Z. Guttenberg, H. Müller, H. Habermüller, A. Geisbauer, J. Pipper, J. Felbel, A. Wixforth, *Lab Chip* **2005**, *5*, 308.
[6] C. Wood, S. Evans, J. Cunningham, R. ORorke, C. Wa lti, A. Davies, *Appl. Phys. Lett.* **2008**, *92*, 044104.
[7] N. D. Orloff, J. R. Dennis, M. Cecchini, E. Schonbrun, E. Rocas, Y. Wang, D. Novotny, R. W. Simmonds, J. Moreland, I. Takeuchi, J. C. Booth, *Biomicrofluidics* **2011**, *5*, 044107.
[8] M. Miansari, A. Qi, L. Y. Yeo, J. R. Friend, *Adv. Funct. Mater.* **2015**, *25*, 989.
[9] S. Shiokawa, Y. Matsui, T. Ueda, *Jpn. J. Appl. Phys.* **1990**, *29*, 137.
[10] M. Kurosawa, A. Futami, T. Higuchi, *Tech. Dig. Solid-State Sens. Actuators* **1997**, *2*, 801.
[11] K. M. Ang, L. Y. Yeo, J. R. Friend, Y. M. Hung, M. K. Tan, *J. Aerosol Sci.* **2015**, *79*, 48.
[12] A. Renaudin, J.-P. Sozanski, B. Verbeke, V. Zhang, P. Tabourier, C. Druon, *Sens. Actuators, B* **2009**, *138*, 374.
[13] M. Travagliati, G. De Simoni, C. M. Lazzarini, V. Piazza, F. Beltram, M. Cecchini, *Lab Chip* **2012**, *12*, 2621.
[14] S. Shiokawa, Y. Matsui, T. Moriizumi, *Jpn. J. Appl. Phys.* **1989**, *28*, 126.
[15] S. Shiokawa, Y. Matsui, T. Ueda, *Proc. IEEE Ultrason. Symp.*, IEEE **1989**, *1*, 643.
[16] M. Cecchini, S. Girardo, D. Pisignano, R. Cingolani, F. Beltram, *Appl. Phys. Lett.* **2008**, *92*, 104103.
[17] L. Masini, M. Cecchini, S. Girardo, R. Cingolani, D. Pisignano, F. Beltram, *Lab Chip* **2010**, *10*, 1997.
[18] R. J. Shilton, M. Travagliati, F. Beltram, M. Cecchini, *Appl. Phys. Lett.* **2014**, *105*, 074106.
[19] M. Dentry, J. Friend, L. Yeo, *Lab Chip* **2014**, *14*, 750.
[20] M. Travagliati, R. J. Shilton, M. Pagliazzi, I. Tonazzini, F. Beltram, M. Cecchini, *Anal. Chem. 86*, 10633.
[21] L. Schmid, A. Wixforth, D. A. Weitz, T. Franke, *Microfluid. Nanofluid.* **2011**, *12*, 229.
[22] A. Renaudin, P. Tabourier, V. Zhang, J. Camart, *Sens. Actuators, B* **2006**, *113*, 389.
[23] R. J. Shilton, N. R. Glass, P. Chan, L. Y. Yeo, J. R. Friend, *Appl. Phys. Lett.* **2011**, *98*, 254103.
[24] N. R. Glass, R. J. Shilton, P. P. Chan, J. R. Friend, L. Y. Yeo, *Small* **2012**, *8*, 1881.
[25] H. Song, D. L. Chen, R. F. Ismagilov, *Angew. Chem. Int. Ed.* **2006**, *45*, 7336.
[26] H. A. Stone, A. D. Stroock, A. Ajdari, *Annu. Rev. Fluid Mech.* **2004**, *36*, 381.
[27] M. Sesen, T. Alan, A. Neild, *Lab Chip* **2014**, *14*, 3325.
[28] D. Collins, T. Alan, K. Helmerson, *A. Neild. Lab Chip* **2013**, *13*, 3225.
[29] T. Franke, A. R. Abate, D. A. Weitz, A. Wixforth, *Lab Chip* **2009**, *9*, 2625.
[30] L. Y. Yeo, J. R. Friend, *Annu. Rev. Fluid Mech.* **2014**, *46*, 379.
[31] J. Kondoh, N. Shimizu, Y. Matsui, M. Sugimoto, S. Shiokawa, *Sens. Actuators, A* **2009**, *149*, 292.
[32] J. Kondoh, N. Shimizu, Y. Matsui, M. Sugimoto, S. Shiokawa, *2005 IEEE Ultrason. Symp.*, IEEE, Rotterdam, Vol. *2*, pp. 1023–1027.
[33] S. Ito, M. Sugimoto, Y. Matsui, J. Kondoh, *Jpn. J. Appl. Phys.* **2007**, *46*, 4718.
[34] D. Beyssen, L. Le Brizoual, O. Elmazria, P. Alnot, I. Perry, D. Maillet, *2006 IEEE Ultrason. Symp.*, IEEE, Vancouver, BC, pp. 949–952.
[35] K. Kulkarni, J. Friend, L. Yeo, P. Perlmutter, *Lab Chip* **2009**, *9*, 754.
[36] T. Roux-Marchand, F. Sarry, D. Beyssen, O. Elmazria, *Ultrason. Symp. (IUS)*, IEEE International (IEEE) **2014**, 1956.
[37] J. Reboud, Y. Bourquin, R. Wilson, G. S. Pall, M. Jiwaji, A. R. Pitt, A. Graham, A. P. Waters, J. M. Cooper, *Proc. Natl. Acad. Sci. USA* **2012**, *109*, 15162.
[38] R. P. Hodgson, M. Tan, L. Yeo, J. Friend, *Appl. Phys. Lett.* **2009**, *94*, 024102.
[39] R. J. Shilton, M. Travagliati, F. Beltram, M. Cecchini, *Adv. Mater.* **2014**, *26*, 4941.
[40] M. Travagliati, R. Shilton, F. Beltram, M. Cecchini, *JoVE* **2013**, e50524.
[41] N.-S. Cheng, *Ind. Eng. Chem. Res.* **2008**, *47*, 3285.
[42] D. Royer, E. Dieulesaint, *Elastic Waves in Solids I: Free and Guided Propagation, Translated by DP Morgan*, Springer-Verlag, New York **2000**.
[43] T. Frommelt, D. Gogel, M. Kostur, P. Talkner, P. Hanggi, A. Wixforth, *IEEE Trans. Ultrasonics, Ferroelectrics, Frequency Control* **2008**, *55*, 2298.
[44] P. Neuzil, C. Zhang, J. Pipper, S. Oh, L. Zhuo, *Nucl. Acids Res.* **2006**, *34*, e77.